Global Journal of Pure and Applied Mathematics.
ISSN 0973-1768 Volume 22, Number 3 (2026), pp. 575–603

https://www.ripublication.com

Modelling Viral Disease Transmission Dynamics with Age and Diabetes Heterogeneity: A Discrete Age-Structured, Diabetes-Stratified SIRD Model

Tejaswi V. Kadam[1] **and Dr. V. R. Nikam**[2]

[1]*Department of Mathematics, L.V.H. Arts, Science and Commerce College, Nashik, India Email: tejaswikadamindia@gmail.com*
[2]*Department of Mathematics, L.V.H. Arts, Science and Commerce College, Nashik, India*

Abstract

A deterministic age- and diabetes-structured compartmental model is developed to investigate the combined effects of age and diabetes on viral disease transmission. The population is divided into four age groups, each stratified into diabetic and non-diabetic susceptible, infectious, recovered, and disease-induced mortality compartments. The model is shown to be well-posed, and the basic reproduction number (R_0) is derived using the next-generation matrix method. Local stability analysis shows that the disease-free equilibrium is stable when $R_0 < 1$ and unstable when $R_0 > 1$. The model is calibrated to COVID-19 data from India (February 2020-February 2021), demonstrating good agreement with reported cases. Numerical simulations and sensitivity analysis identify age-specific transmission and diabetes-related parameters as major drivers of disease spread. The findings highlight the need for targeted interventions for older and diabetic populations and provide a useful framework for evaluating short-term epidemic control strategies.

Keywords. Age-structured model, SIR Model, diabetes heterogeneity, viral disease transmission

2020 Mathematics Subject Classification. Primary 92D30; Secondary 34D20, 37N25.

1. INTRODUCTION

Viral infectious diseases still remain important causes of threat to global public health, economic stability, and healthcare system [1, 2, 3]. The recent epidemics, like the COVID-19 pandemic, have drawn attention to the necessity to study the impact of heterogeneous nature of the population on disease transmission and patient outcomes [4]. Epidemiological research demonstrates that infection susceptibility, disease severity, hospitalization, and mortality differ greatly among demographic and clinical groups of patients [5, 6, 7, 8].

In particular, age and comorbidity conditions became important factors that determine epidemic burden. Diabetes mellitus is among the most important co-morbid conditions identified as major risk factors that lead to poor outcomes from viral infections. Patients with diabetes are known to suffer from weakened immune system, increased susceptibility to infections, longer periods of recovery, and increased chances of developing complications and death [9, 10, 11, 12, 13, 14]. The COVID-19 pandemic witnessed many clinical studies that highlighted high rates of hospitalization and mortality of people with diabetes [15, 16, 17, 18]. Such results were recorded for influenza, SARS, and MERS [19, 20, 21]. Thus, consideration of heterogeneity in the case of diabetes is crucial when using mathematical modeling.

Age, too, is an important determinant of the rate of spread and severity of the disease [22, 23]. The contact structure, social behaviors, immunity, and access to healthcare differ greatly among individuals of different ages [24, 25]. The age-dependent contact patterns can significantly impact the progression of the epidemic and efficiency of any intervention measures taken [26]. This means that the traditional compartmental models of homogeneous mixing will not be sufficient for the examination of complex demographic-disease interactions.

Mathematical epidemiology offers a framework for the study of infectious diseases and assessment of public health interventions [27, 28, 29]. Compartmental models like SIR have been widely used in researching epidemics [30, 31, 32]. The pioneering work of Kermack and McKendrick laid the foundation of deterministic modelling of epidemics, and further studies modified and expanded these models. Age-structured models of epidemics have been extensively studied in the last decades. Many papers took into account age-dependent contact matrices in order to examine heterogeneous contact rates and consider age-targeted interventions [33]. Likewise, models taking into consideration comorbidities and high-risk groups were considered in order to analyze differential epidemic outcomes. In the course of the COVID-19 pandemic, a large number of research works have analyzed the influence of underlying medical conditions, such as diabetes, obesity, cardiovascular diseases, and hypertension, on the development of the epidemic [34, 35].

However, despite these research results, relatively few works have simultaneously considered both age-specific heterogeneity in contacts and risk factors for diabetic people within one model. Models that take into account either only age structure or only comorbidity status of people exist. Consequently, the combined effects of age-specific contact patterns, increased susceptibility among diabetic individuals, reduced recovery rates, and elevated disease-induced mortality remain insufficiently understood.

Motivated by these limitations, the present study develops a deterministic age and diabetes-structured epidemic model for viral disease transmission. The total population is divided into four age groups, each further stratified into diabetic and non-diabetic subpopulations. Individuals in each subgroup are categorized into susceptible, infectious, recovered, and disease-induced mortality compartments. Age-dependent transmission rates are incorporated through a contact matrix, while diabetes-related heterogeneity

is represented by increased susceptibility, reduced recovery rates, and elevated disease-induced mortality. Since the epidemic evolves over a relatively short timescale, demographic processes such as births, natural deaths, aging transitions, and changes in diabetes status are assumed negligible. However, disease-induced mortality is incorporated because disease-related deaths occur on the same timescale as infection and recovery. This modelling approach is particularly appropriate for studying short-term epidemic outbreaks and single-wave scenarios.

The remainder of this paper is organized as follows. Section 2 presents the model formulation, assumptions, and governing equations. Section 3 discusses the basic mathematical characteristics of the proposed model, such as positivity, boundedness, disease-free equilibrium, and basic reproduction number. Section 4 describes how the model is calibrated through the use of data on COVID-19, parameters estimation, goodness-of-fit test, and simulations. Section 5 is devoted to the presentation of a full sensitivity analysis of how increased susceptibility due to diabetes, lower recovery rate due to diabetes, and diabetes prevalence influence the basic reproduction number and epidemic process. Finally, Section 6 provides a summary of results and their epidemiological interpretation.

2. MODEL FORMULATION

We develop a deterministic age- and diabetes-structured compartmental model to investigate the transmission dynamics of a viral disease in a heterogeneous population. The model accounts for differences in disease susceptibility, recovery, and mortality associated with diabetes status, as well as age-dependent contact patterns.
The total population is divided into four age groups indexed by $i = 1, 2, 3, 4$, which may represent children and adolescents, young adults, middle-aged adults, and older adults, respectively. Within each age group, individuals are further stratified according to diabetes status into non-diabetic (ND) and diabetic (D). Each subgroup is partitioned into four epidemiological compartments: susceptible (S); infectious (I); recovered (R); disease-induced deaths (M).Accordingly, the state variables for age group (i) are defined as:
$S_{ND,i}(t),\ I_{ND,i}(t),\ R_{ND,i}(t),\ M_{ND,i}(t)$ and $S_{D,i}(t),\ I_{D,i}(t),\ R_{D,i}(t),\ M_{D,i}(t)$. The total living population in the age group (i) is $N_i(t) = N_{ND,i}(t) + N_{D,i}(t)$, where $N_{ND,i}(t) = S_{ND,i}(t) + I_{ND,i}(t) + R_{ND,i}(t)$ and $N_{D,i}(t) = S_{D,i}(t) + I_{D,i}(t) + R_{D,i}(t)$. The cumulative disease-induced deaths are tracked separately through $M_{ND,i}(t)$ and $M_{D,i}(t)$.

2.1. Model Assumptions

The model is formulated under the following assumptions:

1. The epidemic evolves over a relatively short timescale. So, processes such as births, natural deaths, migration, aging, transition between diabetic and non-diabetic states are neglected.

2. Recovered individuals acquire complete immunity throughout the simulation period.

3. Disease transmission occurs through age-specific contact patterns represented by a transmission matrix.

4. Diabetic individuals have higher susceptibility to infection than non-diabetic individuals, quantified by the susceptibility amplification multiplier $\eta \geq 1$.

5. All infected individuals are equally infectious, regardless of diabetes status.

6. Recovery among diabetic infectives is slower than among non-diabetic infectives and is quantified by the recovery reduction parameter $0 < \delta \leq 1$.

7. Disease-induced mortality is included and may vary by age group and diabetes status, with mortality rates $\mu_{ND,i} \geq 0$ and $\mu_{D,i} \geq 0$ for non-diabetic and diabetic infectives, respectively, where generally $\mu_{D,i} \geq \mu_{ND,i}$.

8. **Force of Infection**
   Let
   $$M = (m_{ij})_{4\times 4}$$
   denote the age-specific contact matrix, where m_{ij} represents the average contact rate between susceptible individuals in age group i and infectious individuals in age group j. The age-specific transmission matrix is defined as
   $$B = (\beta_{ij})_{4\times 4} = cM,$$
   or equivalently,
   $$\beta_{ij} = c\, m_{ij}, \qquad i, j = 1, 2, 3, 4,$$
   where $c > 0$ is transmission probability per effective contact. Thus, β_{ij} represents the effective transmission rate from infectious individuals in age group j to susceptible individuals in age group i, accounting for both the contact frequency and the probability of disease transmission per contact.
   The force of infection experienced by non-diabetic susceptibles in age group (i) is given by
   $$\lambda_{ND,i}(t) = \sum_{j=1}^{4} \beta_{ij} \frac{I_{ND,j}(t) + I_{D,j}(t)}{N_j(t)}, \tag{1}$$
   where
   $$N_j(t) = N_{ND,j}(t) + N_{D,j}(t).$$
   To account for increased susceptibility among diabetic individuals, let $\eta \geq 1$ denote the diabetes-related susceptibility amplification multiplier.
   The force of infection for diabetic susceptibles is defined as
   $$\lambda_{D,i}(t) = \eta \lambda_{ND,i}(t),$$

that is,

$$\lambda_{D,i}(t) = \eta \sum_{j=1}^{4} \beta_{ij} \frac{I_{ND,j}(t) + I_{D,j}(t)}{N_j(t)}. \tag{2}$$

9. **Recovery and Disease-Induced Mortality:** Let $\gamma_{ND,i} > 0$ denote the recovery rate of non-diabetic infectives in age group (i). Recovery among diabetic individuals is assumed to be slower and is modelled by $\gamma_{D,i} = \delta\gamma_{ND,i}$, $0 < \delta \leq 1$, where δ represents the diabetes-related recovery reduction factor.

2.2. Model Diagram

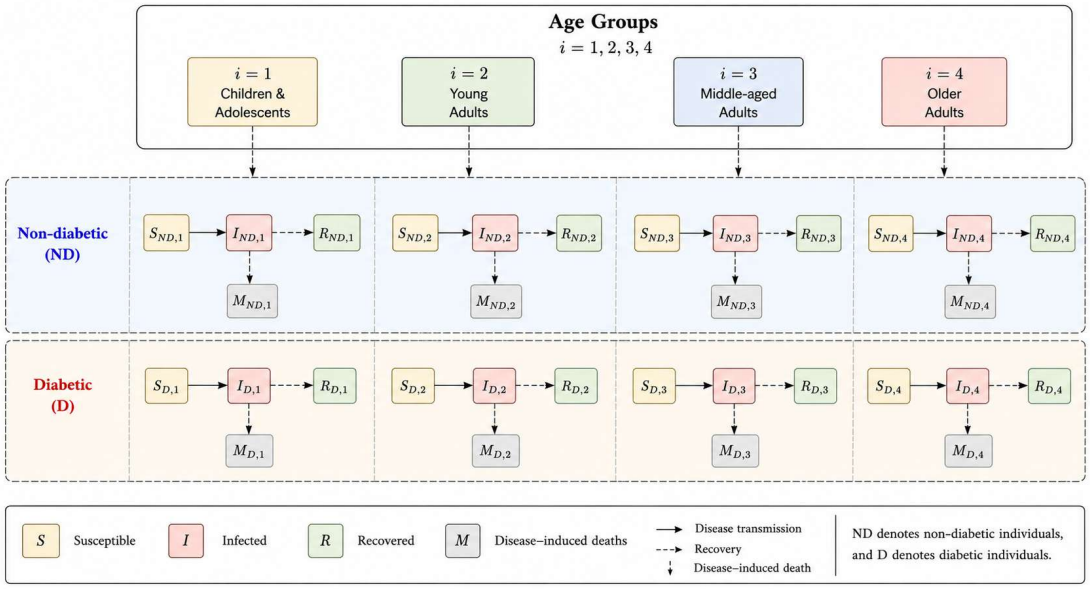

Figure 1: Schematic representation of the proposed age-structured, diabetes-stratified multigroup SIR model with disease-induced mortality.

2.3. Model Equations

For each age group (i=1,2,3,4), the non-diabetic subpopulation satisfies

$$\frac{dS_{ND,i}(t)}{dt} = -\lambda_{ND,i}(t)S_{ND,i}(t) \tag{3}$$

$$\frac{dI_{ND,i}(t)}{dt} = \lambda_{ND,i}(t)S_{ND,i}(t) - (\gamma_{ND,i} + \mu_{ND,i})I_{ND,i}(t) \tag{4}$$

$$\frac{dR_{ND,i}(t)}{dt} = \gamma_{ND,i}I_{ND,i}(t) \tag{5}$$

$$\frac{dM_{ND,i}(t)}{dt} = \mu_{ND,i}I_{ND,i}(t) \tag{6}$$

Similarly, the diabetic subpopulation satisfies

$$\frac{dS_{D,i}(t)}{dt} = -\lambda_{D,i}(t)S_{D,i}(t) \tag{7}$$

$$\frac{dI_{D,i}(t)}{dt} = \lambda_{D,i}(t)S_{D,i}(t) - (\delta\gamma_{ND,i} + \mu_{D,i})I_{D,i}(t) \tag{8}$$

$$\frac{dR_{D,i}(t)}{dt} = \delta\gamma_{ND,i}I_{D,i}(t) \tag{9}$$

$$\frac{dM_{D,i}(t)}{dt} = \mu_{D,i}I_{D,i}(t) \tag{10}$$

Substituting the force of infection terms (1) and (2), yields the complete nonlinear system:

$$\frac{dS_{ND,i}(t)}{dt} = -S_{ND,i}(t)\sum_{j=1}^{4}\beta_{ij}\frac{I_{ND,j}(t) + I_{D,j}(t)}{N_j(t)} \tag{11}$$

$$\frac{dI_{ND,i}(t)}{dt} = S_{ND,i}(t)\sum_{j=1}^{4}\beta_{ij}\frac{I_{ND,j}(t) + I_{D,j}(t)}{N_j(t)} - (\gamma_{ND,i} + \mu_{ND,i})I_{ND,i}(t) \tag{12}$$

$$\frac{dR_{ND,i}(t)}{dt} = \gamma_{ND,i}I_{ND,i}(t) \tag{13}$$

$$\frac{dM_{ND,i}(t)}{dt} = \mu_{ND,i}I_{ND,i}(t) \tag{14}$$

and

$$\frac{dS_{D,i}(t)}{dt} = -\eta S_{D,i}(t)\sum_{j=1}^{4}\beta_{ij}\frac{I_{ND,j}(t) + I_{D,j}(t)}{N_j(t)} \tag{15}$$

$$\frac{dI_{D,i}(t)}{dt} = \eta S_{D,i}(t)\sum_{j=1}^{4}\beta_{ij}\frac{I_{ND,j}(t) + I_{D,j}(t)}{N_j(t)} - (\delta\gamma_{ND,i} + \mu_{D,i})I_{D,i}(t) \tag{16}$$

$$\frac{dR_{D,i}(t)}{dt} = \delta\gamma_{ND,i}I_{D,i}(t) \tag{17}$$

$$\frac{dM_{D,i}(t)}{dt} = \mu_{D,i}I_{D,i}(t) \tag{18}$$

The model is supplemented with the non-negative initial conditions

$$S_{ND,i}(0) = S^0_{ND,i} \geq 0, I_{ND,i}(0) = I^0_{ND,i} \geq 0, R_{ND,i}(0) = R^0_{ND,i} \geq 0, M_{ND,i}(0) = 0,$$

with $N_{ND,i}(0) = S^0_{ND,i} + I^0_{ND,i} + R^0_{ND,i}$

$$S_{D,i}(0) = S^0_{D,i} \geq 0, I_{D,i}(0) = I^0_{D,i} \geq 0, R_{D,i}(0) = R^0_{D,i} \geq 0, M_{D,i}(0) = 0,$$

with $N_{D,i}(0) = S^0_{D,i} + I^0_{D,i} + R^0_{D,i}$.
For all (i=1,2,3,4), the initial living population satisfies $N_i(0) = N_{ND,i}(0) + N_{D,i}(0)$.
The complete model therefore consists of a system of (32) coupled nonlinear ordinary differential equations.

3. MATHEMATICAL ANALYSIS

3.1. Feasible Region, Positivity of Solutions, and Positive Invariance

For each age group $i = 1, 2, 3, 4$, define the living non-diabetic and diabetic populations as

$$N_{ND,i}(t) = S_{ND,i}(t) + I_{ND,i}(t) + R_{ND,i}(t) \; and \; N_{D,i}(t) = S_{D,i}(t) + I_{D,i}(t) + R_{D,i}(t).$$

Since $M_{ND,i}(t)$ and $M_{D,i}(t)$ denote cumulative disease-induced deaths, they are excluded from the living populations. Adding the equations (11),(12),(13) for $S_{ND,i}$, $I_{ND,i}$, and $R_{ND,i}$ yields

$$\frac{dN_{ND,i}(t)}{dt} = \frac{dS_{ND,i}(t)}{dt} + \frac{dI_{ND,i}(t)}{dt} + \frac{dR_{ND,i}(t)}{dt} = -\mu_{ND,i} I_{ND,i}(t).$$

Similarly from (15),(16) & (17),

$$\frac{dN_{D,i}(t)}{dt} = \frac{dS_{D,i}(t)}{dt} + \frac{dI_{D,i}(t)}{dt} + \frac{dR_{D,i}(t)}{dt} = -\mu_{D,i} I_{D,i}(t).$$

Integrating from 0 to t, we obtain

$$N_{ND,i}(t) = N_{ND,i}(0) - \int_0^t \mu_{ND,i} I_{ND,i}(u)\, du,$$

$$N_{D,i}(t) = N_{D,i}(0) - \int_0^t \mu_{D,i} I_{D,i}(u)\, du.$$

Hence, $0 \le N_{ND,i}(t) \le N_{ND,i}(0) \qquad and \qquad 0 \le N_{D,i}(t) \le N_{D,i}(0)$.
Moreover, including the cumulative death compartments gives

$$\frac{d}{dt}\left(N_{ND,i}(t) + M_{ND,i}(t)\right) = -\mu_{ND,i} I_{ND,i}(t) + \mu_{ND,i} I_{ND,i}(t) = 0,$$

$$\frac{d}{dt}\left(N_{D,i}(t) + M_{D,i}(t)\right) = -\mu_{D,i} I_{D,i}(t) + \mu_{D,i} I_{D,i}(t) = 0.$$

Therefore,

$$N_{ND,i}(t) + M_{ND,i}(t) = N_{ND,i}(0), \tag{19}$$

$$N_{D,i}(t) + M_{D,i}(t) = N_{D,i}(0). \tag{20}$$

Consequently, the biologically feasible region is defined by

$$\Omega = \left\{ \begin{array}{l} (S_{ND,i}(t), I_{ND,i}(t), R_{ND,i}(t), M_{ND,i}(t), \\ S_{D,i}(t), I_{D,i}(t), R_{D,i}(t), M_{D,i}(t)) \in \mathbb{R}_+^{32} : \end{array} \right. \tag{21}$$

$$\left. \begin{array}{l} S_{ND,i}(t) + I_{ND,i}(t) + R_{ND,i}(t) + M_{ND,i}(t) = N_{ND,i}(0), \\ S_{D,i}(t) + I_{D,i}(t) + R_{D,i}(t) + M_{D,i}(t) = N_{D,i}(0), \\ i = 1, 2, 3, 4 \end{array} \right\}.$$

Theorem 3.1 (Positivity of Solutions)**.** *Assume that the initial conditions for all epidemiological compartments of both the diabetic and non-diabetic populations are non-negative in each age group. Then every solution of the proposed model remains non-negative for all* $t \geq 0$.

Proof. Given that: For all $i = 1, 2, 3, 4$,

$$S_{ND,i}(0),\ I_{ND,i}(0),\ R_{ND,i}(0),\ M_{ND,i}(0), S_{D,i}(0), I_{D,i}(0),\ R_{D,i}(0),\ M_{D,i}(0) \geq 0.$$

Consider (3), the susceptible non-diabetic compartment:

$$\frac{dS_{ND,i}(t)}{dt} = -\lambda_{ND,i}(t) S_{ND,i}(t),$$

where $\lambda_{ND,i}(t) \geq 0$. Solving explicitly gives

$$S_{ND,i}(t) = S_{ND,i}(0) \exp\left(-\int_0^t \lambda_{ND,i}(u)\, du\right) \geq 0.$$

Similarly, solving (7) gives

$$S_{D,i}(t) = S_{D,i}(0) \exp\left(-\int_0^t \lambda_{D,i}(u)\, du\right) \geq 0.$$

Next, for $I_{ND,i} = 0$, (4) gives

$$\left.\frac{dI_{ND,i}(t)}{dt}\right|_{I_{ND,i}=0} = \lambda_{ND,i}(t) S_{ND,i}(t) \geq 0.$$

Hence, the vector field points inward on the boundary $I_{ND,i} = 0$, implying that $I_{ND,i}(t) \geq 0$. Similarly, for $I_{D,i} = 0$, (8) gives,

$$\left.\frac{dI_{D,i}(t)}{dt}\right|_{I_{D,i}=0} = \lambda_{D,i}(t) S_{D,i}(t) \geq 0,$$

which implies $I_{D,i}(t) \geq 0$.
Furthermore from (5), (6), (9), (10),

$$\frac{dR_{ND,i}(t)}{dt} = \gamma_{ND,i} I_{ND,i}(t) \geq 0, \quad \frac{dR_{D,i}(t)}{dt} = \delta\gamma_{ND,i} I_{D,i}(t) \geq 0,$$
$$\frac{dM_{ND,i}(t)}{dt} = \mu_{ND,i} I_{ND,i}(t) \geq 0, \quad \frac{dM_{D,i}(t)}{dt} = \mu_{D,i} I_{D,i}(t) \geq 0.$$

Since all these derivatives are non-negative whenever the corresponding variables vanish, no solution component can become negative.
Therefore, all state variables remain non-negative for all $t \geq 0$. □

Theorem 3.2 (Positive Invariance)**.** *The feasible region Ω is positively invariant with respect to the flow generated by the model.*

Proof. From the Theorem 3.1, solutions initiating in $\mathbb{R}^{32}_{+}$ remain non-negative for all $t \geq 0$. Moreover,

$$N_{ND,i}(t) + M_{ND,i}(t) = N_{ND,i}(0) \; and \; N_{D,i}(t) + M_{D,i}(t) = N_{D,i}(0).$$

Hence,

$$S_{ND,i}(t) + I_{ND,i}(t) + R_{ND,i}(t) + M_{ND,i}(t) = N_{ND,i}(0),$$

and

$$S_{D,i}(t) + I_{D,i}(t) + R_{D,i}(t) + M_{D,i}(t) = N_{D,i}(0),$$

for all $t \geq 0$ and $i = 1, 2, 3, 4$.
Therefore, every trajectory with initial condition in Ω remains in Ω for all future time. Consequently, Ω is positively invariant. □

3.2. Disease-Free Equilibrium

The disease-free equilibrium (DFE) corresponds to the state in which no infection persists in the population. Hence, all infectious compartments vanish, namely,

$$I_{ND,i} = 0, \qquad I_{D,i} = 0, \qquad i = 1, 2, 3, 4.$$

Since disease-induced mortality occurs only among infectious individuals, it follows that

$$M_{ND,i} = 0, \qquad M_{D,i} = 0, \qquad i = 1, 2, 3, 4.$$

In the absence of infection, the force of infection satisfies

$$\lambda_{ND,i} = 0, \qquad \lambda_{D,i} = 0, \qquad i = 1, 2, 3, 4.$$

Consequently, the governing equations reduce to

$$\frac{dS_{ND,i}}{dt} = 0, \qquad \frac{dR_{ND,i}}{dt} = 0, \qquad \frac{dS_{D,i}}{dt} = 0, \qquad \frac{dR_{D,i}}{dt} = 0.$$

Because the epidemic is assumed to begin in a wholly susceptible population, we take $R_{ND,i} = 0,\ R_{D,i} = 0, \qquad i = 1, 2, 3, 4.$
Using the conservation relations

$$S_{ND,i}(t)+I_{ND,i}(t)+R_{ND,i}(t)+M_{ND,i}(t) = N_{ND,i}(0), \qquad S_{D,i}(t)+I_{D,i}(t)+R_{D,i}(t)+M_{D,i}(t) = N_{D,i}(0)$$

we obtain $S^0_{ND,i} = N_{ND,i}(0), \qquad S^0_{D,i} = N_{D,i}(0).$
Therefore, the disease-free equilibrium is given by

$$E_0 = \Big(N_{ND,1}(0), 0, 0, 0, \ldots, N_{ND,4}(0), 0, 0, 0, \quad N_{D,1}(0), 0, 0, 0, \ldots, N_{D,4}(0), 0, 0, 0\Big). \tag{22}$$

Equivalently,

$$E_0 = \Big(S^0_{ND,1}, 0, 0, 0, \ldots, S^0_{ND,4}, 0, 0, 0, \\ S^0_{D,1}, 0, 0, 0, \ldots, S^0_{D,4}, 0, 0, 0\Big),$$

where

$$S^0_{ND,i} = N_{ND,i}(0), \qquad S^0_{D,i} = N_{D,i}(0), \qquad i = 1, 2, 3, 4.$$

3.3. Basic Reproduction Number

The basic reproduction number, denoted by $\mathcal{R}_0$, is defined as the expected number of secondary infections generated by a typical infectious individual introduced into a wholly susceptible population. We derive $\mathcal{R}_0$ using the next-generation matrix approach developed by [36, 37]. Let the infected-state vector be

$$x = (I_{ND,1}, I_{ND,2}, I_{ND,3}, I_{ND,4}, I_{D,1}, I_{D,2}, I_{D,3}, I_{D,4})^T . \tag{23}$$

For $i = 1, 2, 3, 4$, from (4), (8) the infected compartments satisfy

$$\frac{dI_{ND,i}(t)}{dt} = \lambda_{ND,i}(t)S_{ND,i}(t) - (\gamma_{ND,i} + \mu_{ND,i})I_{ND,i}(t),$$

and

$$\frac{dI_{D,i}(t)}{dt} = \lambda_{D,i}(t)S_{D,i}(t) - (\delta\gamma_{ND,i} + \mu_{D,i})I_{D,i}(t),$$

Following the next-generation matrix method, write the infected subsystem as

$$\frac{dx}{dt} = \mathcal{F}(x) - \mathcal{V}(x), \tag{24}$$

where $\mathcal{F}(x)$ represents the rate of appearance of new infections and $\mathcal{V}(x)$ denotes the rate of transfer between infected compartments.
The vector of new infection terms is

$$\mathcal{F}(x) = \begin{bmatrix} \lambda_{ND,1}S_{ND,1} \\ \lambda_{ND,2}S_{ND,2} \\ \lambda_{ND,3}S_{ND,3} \\ \lambda_{ND,4}S_{ND,4} \\ \lambda_{D,1}S_{D,1} \\ \lambda_{D,2}S_{D,2} \\ \lambda_{D,3}S_{D,3} \\ \lambda_{D,4}S_{D,4} \end{bmatrix}, \tag{25}$$

and the transition vector is

$$\mathcal{V}(x) = \begin{bmatrix} (\gamma_{ND,1} + \mu_{ND,1})I_{ND,1} \\ (\gamma_{ND,2} + \mu_{ND,2})I_{ND,2} \\ (\gamma_{ND,3} + \mu_{ND,3})I_{ND,3} \\ (\gamma_{ND,4} + \mu_{ND,4})I_{ND,4} \\ (\delta\gamma_{ND,1} + \mu_{D,1})I_{D,1} \\ (\delta\gamma_{ND,2} + \mu_{D,2})I_{D,2} \\ (\delta\gamma_{ND,3} + \mu_{D,3})I_{D,3} \\ (\delta\gamma_{ND,4} + \mu_{D,4})I_{D,4} \end{bmatrix}. \tag{26}$$

Evaluating the Jacobian matrices of $\mathcal{F}$ and $\mathcal{V}$ at the disease-free equilibrium Equation (22) yields

$$F = \left[\frac{\partial \mathcal{F}_i}{\partial x_j}(E_0)\right], \qquad V = \left[\frac{\partial \mathcal{V}_i}{\partial x_j}(E_0)\right]. \tag{27}$$

Define the diagonal matrices

$$\Gamma_{ND} = \operatorname{diag}\left(\gamma_{ND,1} + \mu_{ND,1}, \gamma_{ND,2} + \mu_{ND,2}, \gamma_{ND,3} + \mu_{ND,3}, \gamma_{ND,4} + \mu_{ND,4}\right), \tag{28}$$

$$\Gamma_{D} = \operatorname{diag}\left(\delta\gamma_{ND,1} + \mu_{D,1}, \delta\gamma_{ND,2} + \mu_{D,2}, \delta\gamma_{ND,3} + \mu_{D,3}, \delta\gamma_{ND,4} + \mu_{D,4}\right). \tag{29}$$

Let

$$B = (\beta_{ij})_{4\times 4} \tag{30}$$

be the age-specific transmission matrix and define

$$C_{ND} = \operatorname{diag}\left(\frac{S^0_{ND,1}}{N^0_1}, \frac{S^0_{ND,2}}{N^0_2}, \frac{S^0_{ND,3}}{N^0_3}, \frac{S^0_{ND,4}}{N^0_4}\right), \tag{31}$$

and

$$C_{D} = \operatorname{diag}\left(\frac{S^0_{D,1}}{N^0_1}, \frac{S^0_{D,2}}{N^0_2}, \frac{S^0_{D,3}}{N^0_3}, \frac{S^0_{D,4}}{N^0_4}\right), \tag{32}$$

where

$$N^0_i = N_{ND,i}(0) + N_{D,i}(0).$$

The matrix F can then be expressed in block form as

$$F = \begin{bmatrix} C_{ND}B & C_{ND}B \\ \eta C_D B & \eta C_D B \end{bmatrix}, \tag{33}$$

while

$$V = \begin{bmatrix} \Gamma_{ND} & 0 \\ 0 & \Gamma_D \end{bmatrix}. \tag{34}$$

Since V is nonsingular, its inverse is given by

$$V^{-1} = \begin{bmatrix} \Gamma^{-1}_{ND} & 0 \\ 0 & \Gamma^{-1}_{D} \end{bmatrix}. \tag{35}$$

Therefore, the next-generation matrix is

$$K = FV^{-1} = \begin{bmatrix} C_{ND}B\Gamma_{ND}^{-1} & C_{ND}B\Gamma_{D}^{-1} \\ \eta C_D B\Gamma_{ND}^{-1} & \eta C_D B\Gamma_{D}^{-1} \end{bmatrix}. \tag{36}$$

The basic reproduction number is defined as the spectral radius of the next-generation matrix:

$$\mathcal{R}_0 = \rho(FV^{-1}) = \rho(K),$$

where $\rho(\cdot)$ denotes the spectral radius, that is, the maximum modulus of the eigenvalues. Hence,

$$\boxed{\mathcal{R}_0 = \rho\left(\begin{bmatrix} C_{ND}B\Gamma_{ND}^{-1} & C_{ND}B\Gamma_{D}^{-1} \\ \eta C_D B\Gamma_{ND}^{-1} & \eta C_D B\Gamma_{D}^{-1} \end{bmatrix}\right)} \tag{37}$$

The threshold quantity $\mathcal{R}_0$ determines whether the disease can invade the population.

3.4. Local Stability of the Disease-Free Equilibrium

Theorem 3.3. *The disease-free equilibrium E_0 is locally asymptotically stable if $\mathcal{R}_0 < 1$ and unstable if $\mathcal{R}_0 > 1$.*

Proof. The proof follows the next-generation matrix approach of [37]. Let

$$x = (I_{ND,1}, I_{D,1}, I_{ND,2}, I_{D,2}, I_{ND,3}, I_{D,3}, I_{ND,4}, I_{D,4})^T \in \mathbb{R}^8$$

denote the vector of infected compartments.
Let y denote the vector of all uninfected compartments:

$$y = (S_{ND,1}, R_{ND,1}, S_{D,1}, R_{D,1}, \ldots, S_{ND,4}, R_{ND,4}, S_{D,4}, R_{D,4})^T.$$

The full system can be written in the form

$$\frac{dx}{dt} = \mathcal{F}(x, y) - \mathcal{V}(x, y), \tag{38}$$

$$\frac{dy}{dt} = g(x, y), \tag{39}$$

where $\mathcal{F}(x, y)$ is given in Equation (25) contains the rates of appearance of new infections; $\mathcal{V}(x, y)$ as per Equation (26) contains all other transfer terms.
At the disease-free equilibrium $E_0 = (x^*, y^*)$, we have $x^* = 0$. Moreover,

$$S_{ND,i}^* = N_{ND,i}, \qquad S_{D,i}^* = N_{D,i}, \qquad i = 1, 2, 3, 4.$$

Linearizing the infected subsystem about E_0 yields

$$\frac{d\tilde{x}}{dt} = \left[D_x\mathcal{F}(E_0) - D_x\mathcal{V}(E_0)\right]\tilde{x}, \tag{40}$$

where $\tilde{x} = x - x^* = x$. Define

$$F = D_x\mathcal{F}(E_0), \tag{41}$$

$$V = D_x\mathcal{V}(E_0). \tag{42}$$

Hence from Equations (40), (41), (42),

$$\frac{d\tilde{x}}{dt} = (F - V)\tilde{x}.$$

Therefore, the local dynamics of the disease-free equilibrium are determined by the eigenvalues of

$$J = F - V. \tag{43}$$

From Equation (33),

$$F \geq 0,$$

Since it contains only new infection terms.
Moreover, as per Equation (34), V is a nonsingular diagonal matrix with positive entries: Therefore,

$$V^{-1} \geq 0.$$

Consequently,

$$FV^{-1} \geq 0.$$

By the Perron–Frobenius theorem, the non-negative matrix FV^{-1} possesses a dominant real eigenvalue equal to its spectral radius:

$$\mathcal{R}_0 = \rho(FV^{-1}). \tag{44}$$

Let, $s(F - V) = \max\{\mathrm{Re}(\lambda) : \lambda \in \sigma(F - V)\}$ denote the spectral bound of $F - V$, where $\sigma(F - V)$ is the spectrum of $F - V$.
A fundamental result established by van den Driessche and Watmough [37] states that

$$s(F-V) < 0 \iff \rho(FV^{-1}) < 1 \qquad and \qquad s(F-V) > 0 \iff \rho(FV^{-1}) > 1.$$

Therefore from Equation (44),

$$s(F - V) < 0 \iff \mathcal{R}_0 < 1, \tag{45}$$

and

$$s(F - V) > 0 \iff \mathcal{R}_0 > 1. \tag{46}$$

By the linearization theorem [38] for ordinary differential equations,

- if all eigenvalues of the Jacobian have negative real parts, the equilibrium is locally asymptotically stable;
- if at least one eigenvalue has positive real part, the equilibrium is unstable.

Case 1: $\mathcal{R}_0 < 1$**-** From Equation (45), if $\mathcal{R}_0 < 1,$ then $s(F-V) < 0.$
Hence, all eigenvalues of $F - V$ have negative real parts.
Therefore, the disease-free equilibrium E_0 is locally asymptotically stable.
Case 2: $\mathcal{R}_0 > 1$**-** From Equation (46), if $\mathcal{R}_0 > 1,$ $then$ $s(F-V) > 0.$
Hence, $F - V$ possesses at least one eigenvalue with positive real part.
Therefore, the disease-free equilibrium E_0 is unstable.
Thus, $\mathcal{R}_0 < 1 \implies E_0$ is locally asymptotically stable, and
$\mathcal{R}_0 > 1 \implies E_0$ is unstable.
This completes the proof. □

4. NUMERICAL SIMULATION AND MODEL CALIBRATION

To assess the predictive capability of the proposed age- and diabetes-structured SIR model, numerical simulations were performed using the reported COVID-19 infective data for India covering the period from February 2020 to February 2021 [39]. Model calibration was carried out by fitting the model-predicted total infected population to the observed epidemic time series using a nonlinear least-squares optimization procedure implemented in MATLAB. The system of ordinary differential equations was solved numerically using the adaptive Runge–Kutta method through the `ode45` solver. Unless otherwise specified, the baseline parameter values listed in Table 1 were used throughout the simulations. The transmission probability per effective contact c, the diabetes-induced susceptibility multiplier η, and recovery reduction factor δ were estimated during the calibration process by minimizing the discrepancy between the simulated and observed infective populations.

In order to increase the computational efficiency without losing the epidemiological features of the model, demographic data have been normalized to represent a normalized population. Based on demographic and epidemiological estimates for India in 2020-2021, the total population was approximately 1.38×10^9, comprising about 9×10^7 individuals with diabetes and 1.29×10^9 non-diabetic individuals [41, 42]. Instead of employing these large population values directly, which substantially increase computational complexity without affecting the qualitative dynamics, the population was normalized to a total of $13,900$ individuals, consisting of $13,000$ non-diabetic and 900 diabetic individuals. This scaling preserves the relative demographic composition and the proportions of diabetic and non-diabetic subpopulations while enhancing numerical stability and computational efficiency. Since the governing equations are formulated in terms of population interactions and transmission parameters, this normalization does not alter the qualitative disease dynamics, equilibrium behaviour, or the basic reproduction number. Consequently, the simulation results remain representative of the epidemic dynamics in the full population after appropriate rescaling.

The reproduction number $\mathcal{R}_0$ was calculated using the spectral radius of the next generation matrix and it turned out that $\mathcal{R}_0 > 1$, which shows that there is the possibility of sustainable disease transmission. Numerical simulations were then performed in order to study the impact of age structure and diabetes induced heterogeneity on disease transmission.

4.1. Demographic Parameter Assumptions

The total population was partitioned into diabetic and non-diabetic subpopulations with

$$N_{ND} = 13,000, \qquad N_D = 900,$$

respectively. These scaled population sizes were adopted to preserve the demographic structure while ensuring computational efficiency. The non-diabetic population was distributed among four age groups 0-19, 20-39, 40-59, and ≥ 60 years according to the proportions 36%, 33%, 21%, 10% which were derived from the age distribution of the Indian population based on the United Nations World Population Prospects and accessed through the PopulationPyramid.net platform [41, 40]. The diabetic population was distributed as 0.01%, 20%, 35%, 45% reflecting the marked age dependence of diabetes prevalence, with negligible prevalence among children and adolescents and progressively higher prevalence in middle-aged and older adults [42, 43]. These age-specific demographic and epidemiological proportions were selected to be consistent with national population statistics and diabetes prevalence estimates for India and were used to initialize the model for calibration and numerical simulations. Age-dependent contact patterns were incorporated through the contact matrix

$$M = \begin{bmatrix} 2.0 & 0.6 & 0.2 & 0.1 \\ 0.6 & 2.0 & 0.4 & 0.2 \\ 0.2 & 0.4 & 2.0 & 0.5 \\ 0.1 & 0.2 & 0.5 & 2.0 \end{bmatrix},$$

where the diagonal entries exceed the off-diagonal entries, representing more frequent contacts within the same age group than between different age groups. The matrix is a representative assortative mixing matrix whose structure is motivated by empirical studies of human social contacts and age-specific mixing patterns [24, 25, 26]. It is intended to capture the qualitative feature that individuals interact preferentially with others of similar age rather than to reproduce a country-specific contact survey. Such assortative contact patterns have been widely adopted in age-structured epidemic models to describe heterogeneous disease transmission across different age groups [32, 28]. The transmission matrix was defined as

$$\beta_{ij} = cM_{ij},$$

where the transmission probability per effective contact c was estimated from epidemic data during model calibration.

Disease-induced mortality was assumed to increase with age and to be higher among diabetic individuals than among non-diabetic individuals [5, 6, 8]. The daily disease-induced mortality rates were fixed as

$$\mu_{ND} = \left(2 \times 10^{-5},\, 1 \times 10^{-4},\, 8 \times 10^{-4},\, 5 \times 10^{-3}\right)^T \text{ day}^{-1},$$

while the corresponding mortality rates for diabetic individuals were assumed to be 2.5 times larger, i.e.,$\mu_D = 2.5\,\mu_{ND}$.

The selected values are consistent with the well-documented age-related increase in COVID-19 mortality and the higher risk of severe disease and death among individuals with diabetes during the first pandemic wave [5, 13, 15]. Since mortality data were not used for model calibration, disease-induced mortality rates were fixed at epidemiologically plausible values rather than estimated. These values represent a realistic Indian demographic and epidemiological setting. They are used to illustrate the effects of age structure and diabetes heterogeneity on disease transmission rather than to reproduce the exact demographics of a specific population [41, 42, 43].

4.2. Parameter Values Used in Simulations

The demographic, epidemiological, and fitted parameters used in the numerical simulations are summarized in Table 1.

Table 1: Demographic, epidemiological, and fitted parameter values used in the numerical simulations.

Parameter	**Description**	**Value**	**Source**
N_{ND}	Total non-diabetic population	13000	Scaled from [41, 42]
N_D	Total diabetic population	900	Scaled from [41, 42]
$\gamma_{ND,1}$	Recovery rate (0–19 years)	$0.9\ \mathrm{day}^{-1}$	[4, 26]
$\gamma_{ND,2}$	Recovery rate (20–39 years)	$0.7\ \mathrm{day}^{-1}$	[4, 26]
$\gamma_{ND,3}$	Recovery rate (40–59 years)	$0.5\ \mathrm{day}^{-1}$	[4, 6]
$\gamma_{ND,4}$	Recovery rate (60+ years)	$0.3\ \mathrm{day}^{-1}$	[4, 6]
$\mu_{ND,1}$	Disease-induced mortality rate (0-19 years)	$2\times10^{-5}\ \mathrm{day}^{-1}$	Assumed; [5, 8]
$\mu_{ND,2}$	Disease-induced mortality rate (20-39 years)	$1\times10^{-4}\ \mathrm{day}^{-1}$	Assumed; [5, 8]
$\mu_{ND,3}$	Disease-induced mortality rate (40-59 years)	$8\times10^{-4}\ \mathrm{day}^{-1}$	Assumed; [5, 13]
$\mu_{ND,4}$	Disease-induced mortality rate (60+ years)	$5\times10^{-3}\ \mathrm{day}^{-1}$	Assumed; [5, 13]
κ	Diabetes mortality multiplier	2.5	Based on [13, 15]
$I_{ND,2}(0)$	Initial infectives (non-diabetic)	1	Fixed
$I_{D,2}(0)$	Initial infectives (diabetic)	0	Fixed
c	Transmission probability per effective contact	Estimated	Model calibration
η	Diabetes-induced susceptibility amplification multiplier	Estimated	Model calibration
δ	Diabetes-induced recovery reduction factor	Estimated	Model calibration

4.3. Model Calibration and Data Fitting

The model was first calibrated to the observed epidemic data in order to assess its ability to reproduce the observed transmission dynamics. Figure 2 compares the observed

infective population with the model-predicted total infected population obtained from parameter estimation.

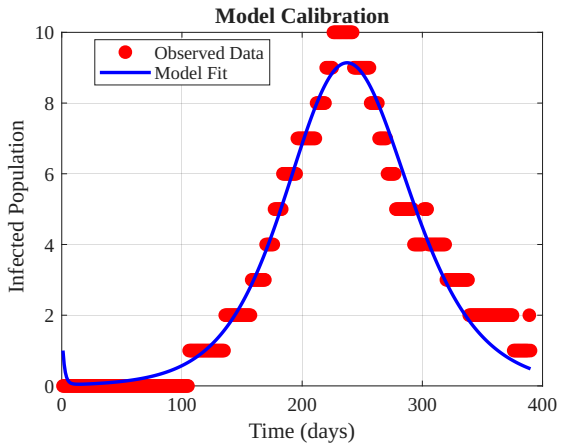

Figure 2: Comparison between the reported COVID-19 infective data and the model-predicted total infected population obtained from parameter estimation.

The fitted epidemic trajectory closely follows the observed data and successfully captures the main characteristics of the outbreak, including the initial growth phase, epidemic peak, and subsequent decline. The agreement between the observed and simulated curves demonstrates that the proposed age- and diabetes-structured framework provides a satisfactory description of the epidemic dynamics.

To further examine the contribution of different age groups, Figure 3 presents the age-specific infected populations reconstructed from the fitted model. Distinct epidemic patterns are observed across age groups due to heterogeneous contact patterns and differences in diabetes prevalence. In particular, older age groups exhibit larger infection burdens, indicating their greater contribution to overall disease transmission.

4.4. Parameter Estimation

The unknown parameters c, η, and δ were estimated by fitting the model-predicted infective population to the reported COVID-19 infective data from February 2020 to February 2021 using the MATLAB nonlinear least-squares routine `lsqcurvefit`. The estimated parameter values are summarized in Table 2. The estimated value $\eta = 6.0835$

Table 2: Estimated model parameters.

Parameter	Description	Estimated Value
c	Transmission probability per effective contact	0.055451
η	Diabetes susceptibility multiplier	6.083507
δ	Recovery reduction factor	0.615443

indicates that diabetic individuals are substantially more susceptible to infection than

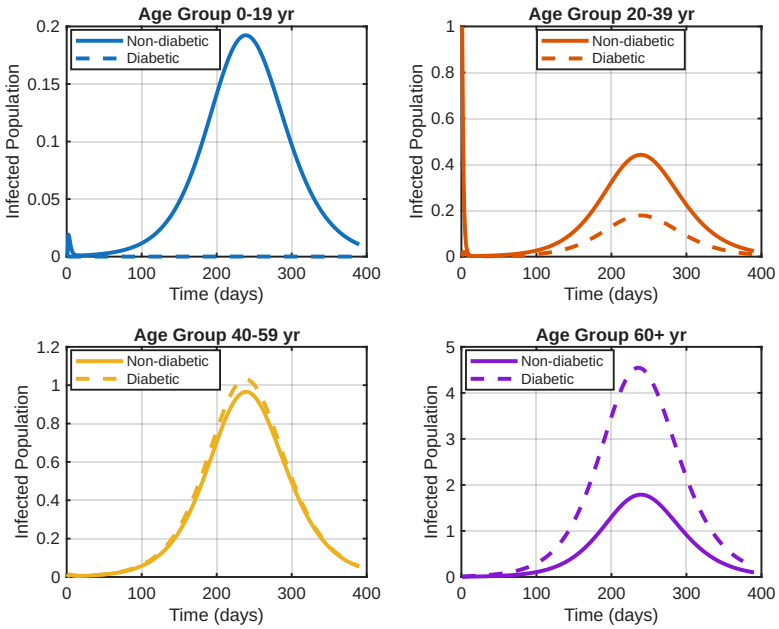

Figure 3: Age-specific infected populations predicted by the calibrated age- and diabetes-structured model.

non-diabetic individuals. Furthermore, $\delta = 0.6154$ implies that diabetic individuals recover at approximately 61% of the recovery rate of their non-diabetic counterparts, resulting in prolonged infectious periods and enhanced disease transmission.

4.5. Goodness-of-Fit Analysis

The calibrated model closely reproduces the observed epidemic trajectory. The goodness-of-fit statistics obtained from the calibration procedure are

$$\text{SSE} = 122.537672, \tag{47}$$

$$\text{RMSE} = 0.560535, \tag{48}$$

$$R^2 = 0.967451. \tag{49}$$

The coefficient of determination ($R^2 = 0.9675$) indicates that approximately 96.8% of the variability in the observed infective data is explained by the model. The relatively small RMSE further confirms the excellent agreement between model predictions and reported COVID-19 data, demonstrating the suitability of the proposed age- and diabetes-structured framework for capturing epidemic dynamics.

4.6. Simulation Results

Using the estimated parameter values, the basic reproduction number was computed through the next-generation matrix approach, yielding

$$R_0 = 1.135805. \tag{50}$$

Since $R_0 > 1$, the disease-free equilibrium is unstable and sustained disease transmission is possible within the population. The numerical simulations reveal that diabetes significantly influences disease dynamics. The large estimated susceptibility multiplier ($\eta = 6.0835$) indicates that diabetic individuals contribute disproportionately to the spread of infection. Moreover, the reduced recovery rate associated with diabetes ($\delta = 0.6154$) prolongs the infectious period, resulting in higher infection prevalence among diabetic age groups.

The calibrated model successfully reproduces the observed COVID-19 epidemic curve while simultaneously capturing age-specific and diabetes-related heterogeneity. These findings highlight the importance of targeted intervention strategies aimed at high-risk diabetic populations, particularly within older age groups, to effectively mitigate disease transmission and reduce the overall epidemic burden.

5. SENSITIVITY ANALYSIS OF DIABETES-RELATED PARAMETERS

To quantify the influence of diabetes-related epidemiological factors on disease transmission, a sensitivity analysis was performed by varying the diabetes susceptibility multiplier (η), recovery reduction factor (δ), and diabetic population proportion while keeping all other parameters fixed at their calibrated or assumed values in simulation as given in Table 1. The analysis focused on changes in the basic reproduction number (R_0) and the resulting dynamics of the infected population.

The baseline calibrated parameter values obtained from model fitting to COVID-19 infective data (February 2020-February 2021) and parameter ranges used for sensitivity analysis are presented in Table 3.

Table 3: Baseline Parameter Values and Parameter Ranges considered in sensitivity analysis.

Parameter	Baseline Value	Range Investigated
η	6.0835	2, 4, 6, 8, 10
δ	0.6154	0.2, 0.4, 0.6, 0.8, 1.0
Diabetic population proportion	6.47%	5%, 7%, 10%, 20%, 40%

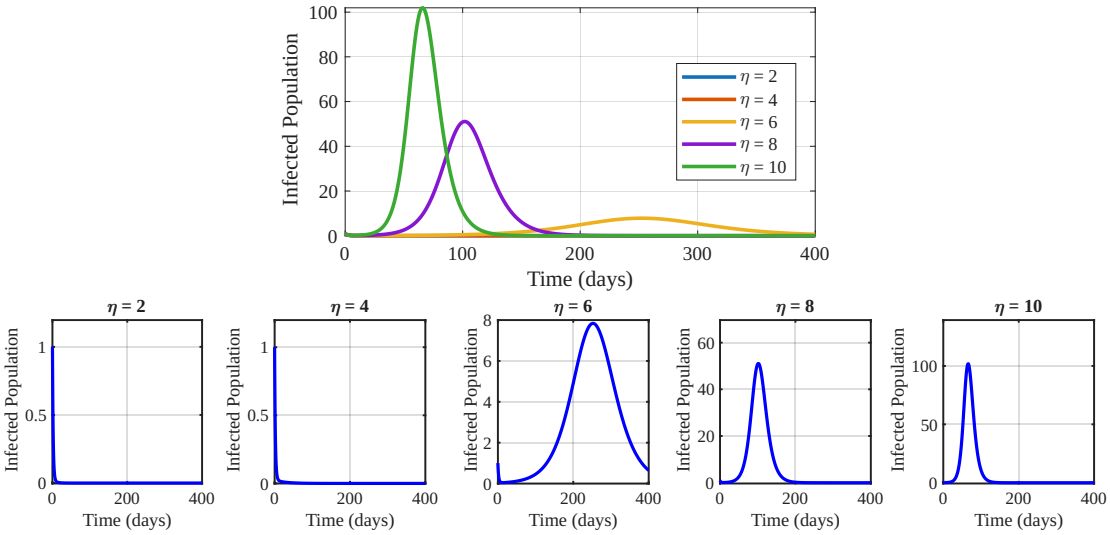

Figure 4: Effect of the diabetes susceptibility multiplier η on the epidemic dynamics.

5.1. Sensitivity of Infective Dynamics and R_0 to Diabetes Susceptibility Multiplier (η)

5.1.1. Effect of the Diabetes Susceptibility Multiplier η on Disease Dynamics

To examine the effect of diabetes-related susceptibility on disease transmission, the susceptibility multiplier η was varied while all other parameters were fixed at their baseline values (Figure 4). Increasing η markedly intensified disease transmission. Lower values (η=2,4) produced negligible outbreaks, whereas higher values (η=6,8,10) resulted in progressively larger epidemic peaks occurring earlier, with η=10 producing the largest outbreak. Figure 5 shows the corresponding age-specific infective dynamics. Increasing η increased the epidemic burden across all age groups, with larger and earlier epidemic peaks. The oldest age group (Age Group 4) experienced the highest infection peak, followed by Age Groups 3, 2, and 1. These results suggest that reducing susceptibility among individuals with diabetes can substantially mitigate disease transmission, particularly in older populations.

5.1.2. Effect of the Diabetes Susceptibility Multiplier η on the Basic Reproduction Number

Figure 6 shows that the basic reproduction number, $\mathcal{R}_0$, increases monotonically with the diabetes susceptibility multiplier, η. As η increases from 2 to 10, $\mathcal{R}_0$ rises from approximately 0.58 to 1.67, crossing the epidemic threshold. This indicates that greater diabetes-related susceptibility promotes sustained disease transmission.
Overall, the simulations show that the diabetes susceptibility multiplier, η, strongly influences disease transmission. Higher η produces larger and earlier epidemic peaks, increases $\mathcal{R}_0$ beyond the epidemic threshold, and has the greatest impact on older age

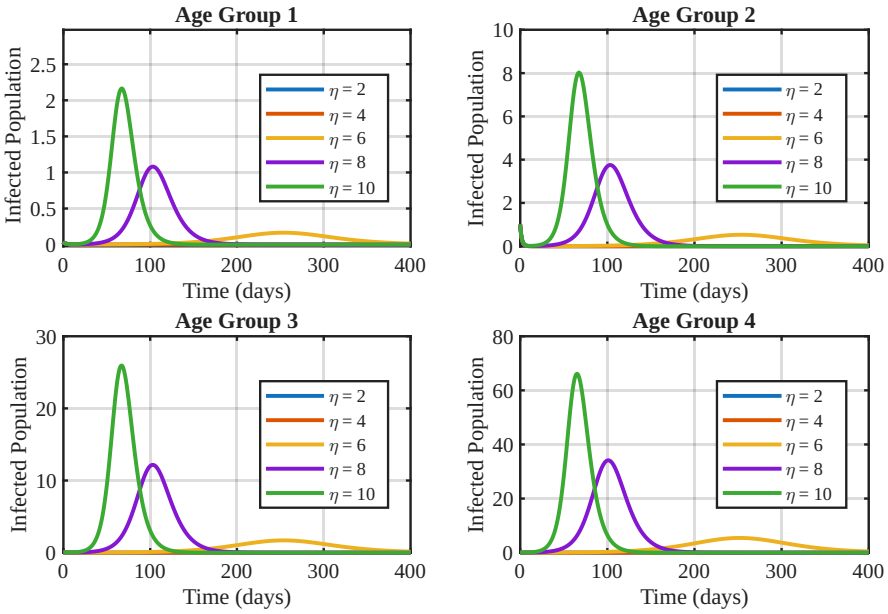

Figure 5: Effect of η on age-group wise epidemic dynamics

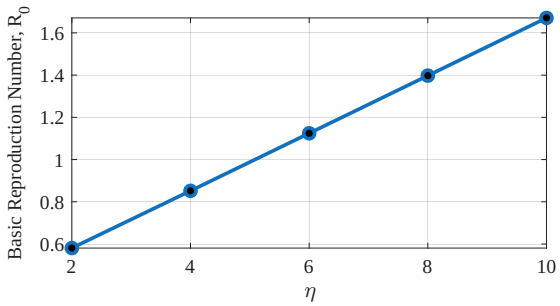

Figure 6: Effect of η on the basic reproduction number $\mathcal{R}_0$.

groups. Reducing susceptibility among individuals with diabetes through effective prevention and control measures can substantially reduce disease transmission and epidemic burden.

5.2. Sensitivity of R_0 and Infective Dynamics to Recovery Reduction Factor (δ)

5.2.1. Effect of the Recovery Reduction Factor δ on Disease Dynamics

The recovery reduction factor, δ, represents the recovery rate of diabetic individuals relative to non-diabetic individuals. To assess its effect, δ was varied while all other parameters were fixed (Figure 7). Lower values ($\delta = 0.2$) produced large, early epidemic peaks due to slower recovery, whereas increasing δ reduced and delayed the epidemic. For $\delta = 0.8$ and 1.0, the epidemic remained negligible. Figure 8 shows the corresponding age-specific dynamics. Lower δ resulted in the highest infective burden across all age

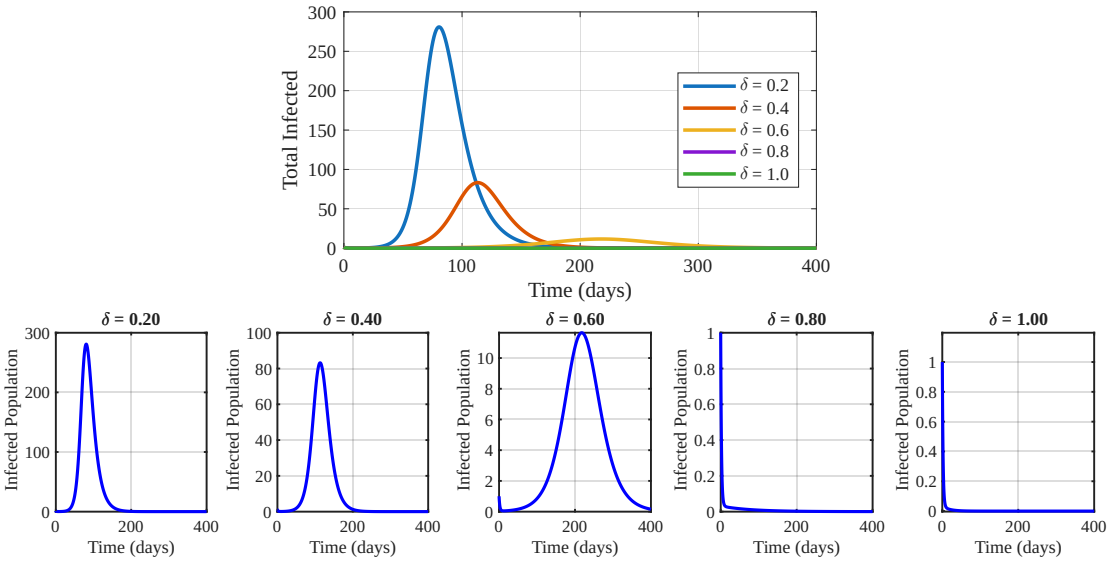

Figure 7: Effect of δ on epidemic dynamics

groups, particularly in the oldest group (Age Group 4). As δ increased, epidemic peaks decreased markedly and occurred later, with negligible infections for $\delta = 0.8$ and 1.0.

These results indicate that improving recovery among diabetic individuals can substantially reduce disease transmission, especially in older age groups.

5.2.2. Effect of the Recovery Reduction Factor δ on the Basic Reproduction Number.

Figure 9 shows that the basic reproduction number, $\mathcal{R}_0$, decreases monotonically as the recovery reduction factor, δ, increases. $\mathcal{R}_0$ declines from approximately 2.57 at $\delta = 0.2$ to 0.83 at $\delta = 1.0$, falling below the epidemic threshold. This indicates that faster recovery of diabetic individuals can prevent sustained disease transmission.
Overall, increasing δ reduces epidemic peaks, shortens the infectious period, and lowers $\mathcal{R}_0$. These findings highlight the importance of timely diagnosis, effective treatment, and improved clinical management of diabetic individuals in reducing disease transmission and epidemic burden.

5.3. Sensitivity of Disease Dynamics to Diabetic Prevalence

To investigate the effect of diabetes prevalence, the proportion of diabetic individuals was varied from 5% to 40% while all other parameters were fixed (Figure 10). Increasing diabetes prevalence markedly intensified disease transmission. Low prevalence (5% and 7%) produced small outbreaks, whereas higher prevalence (10%-40%) resulted in progressively larger epidemic peaks occurring earlier. These results indicate that higher diabetes prevalence accelerates epidemic progression and increases the infective

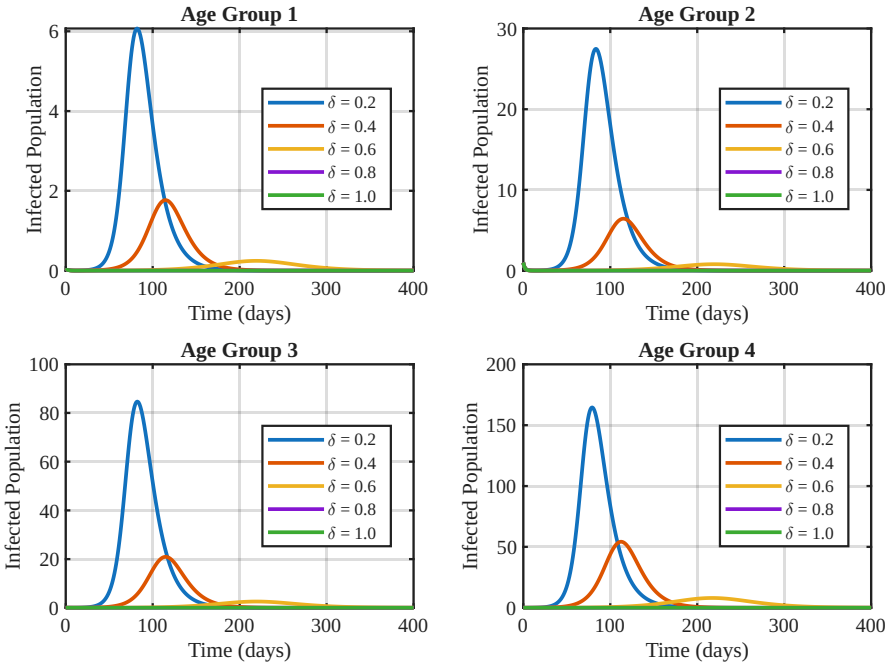

Figure 8: Effect of δ on Age-group wise epidemic dynamics.

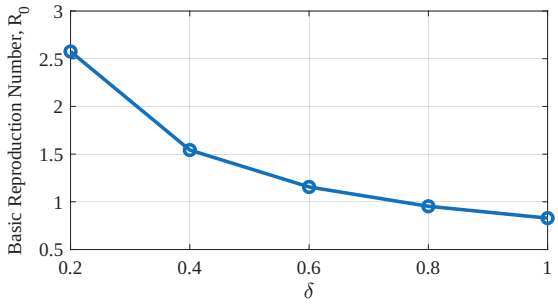

Figure 9: Effect of δ on the basic reproduction number $\mathcal{R}_0$

burden. Overall, the simulations show that higher diabetes prevalence leads to larger and earlier epidemic outbreaks, accelerating disease transmission. These findings highlight the importance of diabetes prevention, effective management, vaccination, early diagnosis, and appropriate clinical care to reduce disease transmission and epidemic burden, particularly in high-risk populations.

6. CONCLUSION

This study presents an age- and diabetes-structured SIR epidemic model with disease-induced death to investigate the role of demographic diversity and diabetes co-morbidity on the spread of the disease. In this regard, the population is subdivided into four age classes, which are further classified into diabetics and non-diabetics. Various properties of the model were derived based on the generation matrix approach, including positivity, boundedness, and stability of the disease-free equilibrium. The

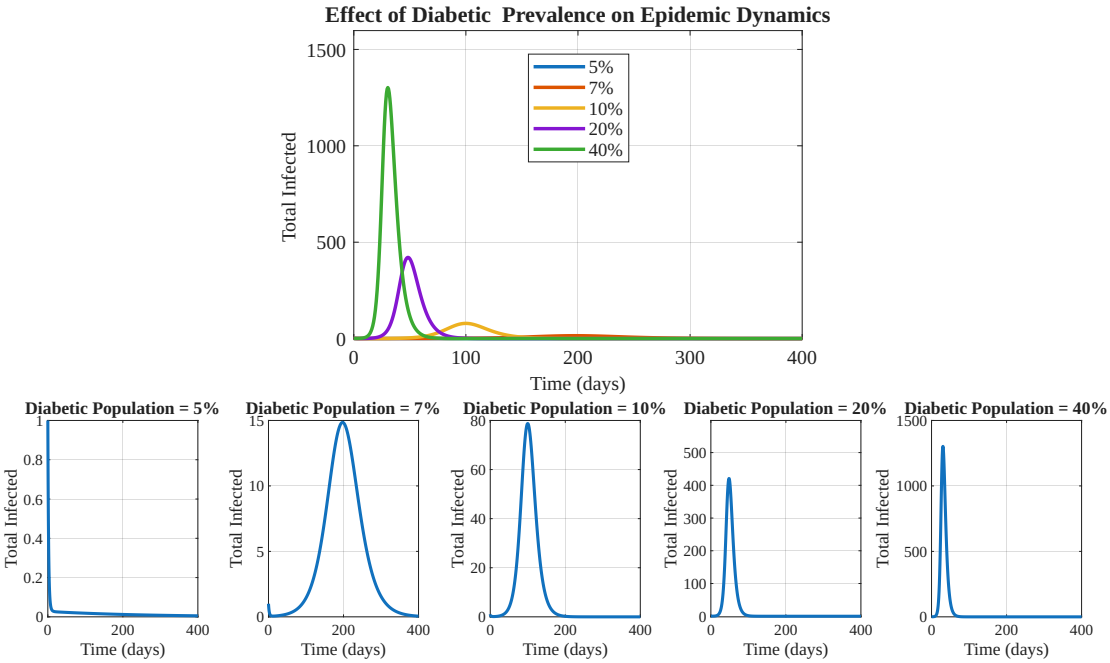

Figure 10: Effect of Diabetes Prevalence on epidemic dynamics

model has been fitted based on reported data of the COVID-19 epidemic outbreak in India from February 2020 to February 2021, and the simulated infected cases are well in line with the data, confirming that the model can capture the first wave dynamics.

Numerical simulations highlighted the impact of diabetes-related factors on disease transmission. Increasing the diabetes susceptibility multiplier (η) resulted in larger epidemic peaks and a higher basic reproduction number ($\mathcal{R}_0$). Decreasing η suppressed transmission and delayed epidemic peaks.

On the other hand, increasing the recovery reduction factor (δ) enhanced the recovery of diabetic individuals, resulting in smaller epidemic peaks and a reduction in $\mathcal{R}_0$, while decreasing δ prolonged the infectious period, intensified disease transmission, and increased the epidemic burden. Similarly, increasing the proportion of diabetic individuals in the population produced larger and earlier epidemic outbreaks. Age-specific simulations showed that older groups experienced the highest disease burden.

Overall, the findings demonstrate that diabetes is an important epidemiological risk factor influencing both the magnitude and persistence of COVID-19 transmission. The proposed model suggests that interventions aimed at reducing infection susceptibility and improving recovery among diabetic individuals, together with effective diabetes management, vaccination, and timely clinical care, can substantially mitigate disease transmission and reduce the overall epidemic burden.

The modelling framework developed in this study provides a useful tool for assessing the impact of chronic comorbidities on infectious disease dynamics and may assist public

health authorities in designing targeted intervention strategies for high-risk populations.

The present model can be extended in several directions. Future work may incorporate vaccination, waning immunity, stochastic effects, spatial heterogeneity, optimal control strategies, or additional comorbidities such as hypertension and obesity. Such extensions would provide a more comprehensive framework for understanding the interaction between chronic diseases and emerging infectious diseases and support the development of more effective public health policies.

REFERENCES

[1] Nature Reviews Microbiology. (2026). Evolving viral threats. *Nature Reviews Microbiology*, *24*, 1–2. https://doi.org/10.1038/s41579-025-01263-x

[2] Drotman, D. (2025). "Terrifying and Boring"—Reflecting on 30 years of Emerging Infectious Diseases. *Emerging Infectious Diseases*, *31*(12), 2347–2348. https://doi.org/10.3201/eid3112.ac3112

[3] IHME Pathogen Core Group. (2024). Global burden associated with 85 pathogens in 2019: A systematic analysis for the Global Burden of Disease Study 2019. *The Lancet Infectious Diseases*, *24*(8), 868–895. https://doi.org/10.1016/S1473-3099(24)00158-0

[4] World Health Organization. (2023). *COVID-19 Epidemiological Update*. World Health Organization. https://www.who.int/emergencies/diseases/novel-coronavirus-2019

[5] Williamson, E. J., Walker, A. J., Bhaskaran, K., et al. (2020). Factors associated with COVID-19-related death using OpenSAFELY. *Nature*, *584*, 430–436. https://doi.org/10.1038/s41586-020-2521-4

[6] Brodin, P. (2021). Immune determinants of COVID-19 disease presentation and severity. *Nature Medicine*, *27*, 28–33. https://doi.org/10.1038/s41591-020-01202-8

[7] The COVID-19 Host Genetics Initiative. (2023). A second update on mapping the human genetic architecture of COVID-19. *Nature*, *621*, E7–E26. https://doi.org/10.1038/s41586-023-06355-3

[8] Clark, A., Jit, M., Warren-Gash, C., et al. (2020). Global, regional, and national estimates of the population at increased risk of severe COVID-19 due to underlying health conditions in 2020: A modelling study. *The Lancet Global Health*, *8*(8), e1003–e1017. https://doi.org/10.1016/S2214-109X(20)30264-3

[9] Geerlings, S. E., & Hoepelman, A. I. M. (1999). Immune dysfunction in patients with diabetes mellitus (DM). *FEMS Immunology & Medical Microbiology*, *26*(3–4), 259–265. https://doi.org/10.1111/j.1574-695X.1999.tb01397.x

[10] Unnikrishnan, R., & Misra, A. (2020). Infections and diabetes: Risks and mitigation with reference to India. *Diabetes & Metabolic Syndrome: Clinical Research &*

Reviews, *14*(6), 1889–1894. https://doi.org/10.1016/j.dsx.2020.09.022

[11] Wensveen, T. T., Gašparini, D., Rahelić, D., & Wensveen, F. M. (2021). Type 2 diabetes and viral infection: Cause and effect of disease. *Diabetes Research and Clinical Practice*, *172*, Article 108637. https://doi.org/10.1016/j.diabres.2020.108637

[12] Ambati, S. K. (2020). Compromised immune response to viral infections in type 2 diabetes mellitus. *International Journal of Community Medicine and Public Health*, *7*(12), 5203–5207. https://doi.org/10.18203/2394-6040.ijcmph20205274

[13] Apicella, M., Campopiano, M. C., Mantuano, M., Mazoni, L., Coppelli, A., & Del Prato, S. (2020). COVID-19 in people with diabetes: Understanding the reasons for worse outcomes. *The Lancet Diabetes & Endocrinology*, *8*(9), 782–792. https://doi.org/10.1016/S2213-8587(20)30238-2

[14] Joshi, G., Das, A., Verma, G., & Guchhait, P. (2024). Viral infection and host immune response in diabetes. *IUBMB Life*, *76*(5), 242–266. https://doi.org/10.1002/iub.2794

[15] Fatoke, B., Hui, A. L., Saqib, M., et al. (2025). Type 2 diabetes mellitus as a predictor of severe outcomes in COVID-19—A systematic review and meta-analysis. *BMC Infectious Diseases*, *25*, Article 719. https://doi.org/10.1186/s12879-025-11089-w

[16] Wu, J., Zhang, J., Sun, X., Wang, L., Xu, Y., Zhang, Y., Liu, X., & Dong, C. (2020). Influence of diabetes mellitus on the severity and fatality of SARS-CoV-2 (COVID-19) infection. *Diabetes, Obesity and Metabolism*, *22*(10), 1907–1914. https://doi.org/10.1111/dom.14105

[17] Huang, I., Lim, M. A., & Pranata, R. (2020). Diabetes mellitus is associated with increased mortality and severity of disease in COVID-19 pneumonia: A systematic review, meta-analysis, and meta-regression. *Diabetes & Metabolic Syndrome: Clinical Research & Reviews*, *14*(4), 395–403. https://doi.org/10.1016/j.dsx.2020.04.018

[18] Nazumulkani, A., & Ali, A. S. (2025). The impact of type 2 diabetes mellitus on the severity of influenza infection: A single-centre retrospective observational study from India. *Apollo Medicine*, Advance online publication. https://doi.org/10.1177/09760016251365084

[19] Fang, M., Ishigami, J., Echouffo-Tcheugui, J. B., et al. (2021). Diabetes and the risk of hospitalisation for infection: The Atherosclerosis Risk in Communities (ARIC) study. *Diabetologia*, *64*, 2458–2465. https://doi.org/10.1007/s00125-021-05522-3

[20] Kjölhede, E. A., Carlsen, H. K., Martyn, O., et al. (2025). Hospitalisation from seasonal influenza among persons with type 1 diabetes: A cohort study from the Swedish National Diabetes Register. *BMJ Open*, *15*, Article e084165. https://doi.org/10.1136/bmjopen-2024-084165

[21] Yang, J. K., Feng, Y., Yuan, M. Y., et al. (2006). Plasma glucose levels and diabetes are independent predictors for mortality and morbidity in patients with SARS. *Diabetics Medicine*, *23*(6), 623–628. https://doi.org/10.1111/j.1464-5491.2006.01861.x

[22] Leng, J., & Goldstein, D. R. (2010). Impact of aging on viral infections. *Microbes and Infection*, *12*(14–15), 1120–1124. https://doi.org/10.1016/j.micinf.2010.08.009

[23] Møgelmose, S., Neels, K., Beutels, P., et al. (2023). Exploring the impact of population ageing on the spread of emerging respiratory infections and the associated burden of mortality. *BMC Infectious Diseases*, *23*, Article 767. https://doi.org/10.1186/s12879-023-08657-3

[24] Mossong, J., Hens, N., Jit, M., Beutels, P., Auranen, K., Mikolajczyk, R., Massari, M., Salmaso, S., Tomba, G. S., Wallinga, J., Heijne, J., Sadkowska-Todys, M., Rosinska, M., & Edmunds, W. J. (2008). Social contacts and mixing patterns relevant to the spread of infectious diseases. *PLoS Medicine*, *5*(3), e74. https://doi.org/10.1371/journal.pmed.0050074

[25] Prem, K., Cook, A. R., & Jit, M. (2021). Projecting social contact matrices in 177 geographical regions: An update and comparison with empirical data for the COVID-19 era. *PLoS Computational Biology*, *17*(7), e1009098. https://doi.org/10.1371/journal.pcbi.1009098

[26] Davies, N. G., Klepac, P., Liu, Y., Prem, K., Jit, M., & Eggo, R. M. (2020). Age-dependent effects in the transmission and control of COVID-19 epidemics. *Nature Medicine*, *26*, 1205–1211. https://doi.org/10.1038/s41591-020-0962-9

[27] Brauer, F. (Ed.). (2019). *Mathematical Epidemiology*. Springer. https://doi.org/10.1007/978-3-030-23413-7

[28] Martcheva, M. (2015). *An Introduction to Mathematical Epidemiology*. Texts in Applied Mathematics, Vol. 61. New York, NY: Springer. https://doi.org/10.1007/978-1-4899-7612-3

[29] Diekmann, O., Heesterbeek, H., & Britton, T. (2013). *Mathematical Tools for Understanding Infectious Disease Dynamics*. Princeton University Press.

[30] Kermack, W. O., & McKendrick, A. G. (1927). A contribution to the mathematical theory of epidemics. *Proceedings of the Royal Society A: Mathematical, Physical and Engineering Sciences*, *115*(772), 700–721. https://doi.org/10.1098/rspa.1927.0118

[31] Hethcote, H. W. (2000). The mathematics of infectious diseases. *SIAM Review*, *42*(4), 599–653. https://doi.org/10.1137/S0036144500371907

[32] Keeling, M. J., & Rohani, P. (2008). *Modeling Infectious Diseases in Humans and Animals*. Princeton University Press.

[33] Upadhyay, R. K., Chatterjee, S., Saha, S., & Azad, R. K. (2020). Age-group-targeted testing for COVID-19 as a new prevention strategy.

Nonlinear Dynamics, *101*(3), 1921–1932. https://doi.org/10.1007/s11071-020-05879-x

[34] Das, P., Upadhyay, R. K., Misra, A. K., Rihan, F. A., Das, P., & Ghosh, D. (2021). Mathematical model of COVID-19 with comorbidity and controlling using non-pharmaceutical interventions and vaccination. *Nonlinear Dynamics*, *106*(2), 1213–1227. https://doi.org/10.1007/s11071-021-06517-w

[35] Das, P., Nadim, S. S., Das, S., & Das, P. (2021). Dynamics of COVID-19 transmission with comorbidity: A data-driven modelling based approach. *Nonlinear Dynamics*, *106*(2), 1197–1211. https://doi.org/10.1007/s11071-021-06324-3

[36] Diekmann, O., Heesterbeek, J. A. P., & Metz, J. A. J. (1990). On the definition and the computation of the basic reproduction ratio R_0 in models for infectious diseases in heterogeneous populations. *Journal of Mathematical Biology*, *28*(4), 365–382. https://doi.org/10.1007/BF00178324

[37] van den Driessche, P., & Watmough, J. (2002). Reproduction numbers and sub-threshold endemic equilibria for compartmental models of disease transmission. *Mathematical Biosciences*, *180*, 29–48. https://doi.org/10.1016/S0025-5564(02)00108-6

[38] Perko, L. (2001). *Differential Equations and Dynamical Systems* (3rd ed.). Springer, New York. https://doi.org/10.1007/978-1-4613-0003-8

[39] COVID19India.org. (2021). *COVID-19 India Data Repository: Time Series and State-wise Data*. COVID19India.org. https://data.covid19india.org/

[40] PopulationPyramid.net. (2025). *Population Pyramids of the World from 1950 to 2100*. Retrieved from https://www.populationpyramid.net/

[41] United Nations, Department of Economic and Social Affairs, Population Division. (2022). *World Population Prospects 2022*. United Nations. https://population.un.org/wpp/

[42] International Diabetes Federation. (2021). *IDF Diabetes Atlas* (10th ed.). Brussels, Belgium: International Diabetes Federation. https://diabetesatlas.org/

[43] Anjana, R. M., Deepa, M., Pradeepa, R., et al. (2023). Prevalence of diabetes and prediabetes in 15 states of India: Results from the ICMR–INDIAB population-based cross-sectional study. *The Lancet Diabetes & Endocrinology*, *11*(7), 473–481. https://doi.org/10.1016/S2213-8587(23)00138-0